# Supporting information

## Supramolecular DNA photonic hydrogels for on demand control of coloration with high spatial and temporal resolution

*Authors: Yixiao Dong, J. Dale Combs, Cong Cao, Eric R. Weeks, Alisina Bazrafshan, SK Aysha Rashid, Khalid Salaita**

Address:
Y. Dong, J. Dale Combs, A. Bazrafshan, SK A. Rashid, K. Salaita
Department of Chemistry, Emory University, 1515 Dickey Drive, Atlanta, Georgia 30322, United States

C.Cao, E. R. Weeks
Department of Physics, Emory University, 400 Dowman Drive Atlanta, Georgia 30322, United States
*Corresponding author: k.salaita@emory.edu

**Materials and methods**

All chemicals were purchased from Millipore Sigma unless noted otherwise. All DNA strands are custom synthesized by Integrated DNA Technologies (Coralville, IA). The DNA sequences are listed in **Figure 2** in the main text.

1) Synthesis of $Fe_3O_4$ nanoparticles

The protocols for the synthesis of MNPs was adapted from our previously published work[1]. Briefly, 0.65 g $FeCl_3$, 40 mL ethylene glycol, 3.0 g sodium ascorbate, 1.05 g Poly(4-styrenesulfonic acid-co-maleic acid) sodium salt ($M_w$~20,000; 1:1 4-styrenesulfonic acid:maleic acid mole ratio), 14 mg D-isoascorbic acid, and 120 μL DI $H_2O$ were added consecutively into a beaker sealed by parafilm. After vigorous magnetic stirring for about 40 min, a homogeneous mixture was formed and then 0.6 g NaOH was added. The mixture was stirred for 1-2 h until all the NaOH pellets were dissolved completely. The mixture was then transferred into a capped 50 mL Erlenmeyer flask and then allowed to react in a preheated oven (190 ˚C) for 9 h. The $Fe_3O_4$ products were separated from the solution using an external rare-earth (NdFeB) magnet and washed. Initially, the particles were washed with 30 mL of 50% ethanol solution three times, and then washed three additional times with DI water. To generate smaller (~100 nm) and larger (~130 nm) sizes of nanoparticles (shown in **Figure S1**), we tuned the amount of added water to 180 μL and 110 μL, respectively.

2) Synthesis of $Fe_3O_4$@$SiO_2$ nanoparticles

The as-synthesized magnetite particles were re-dispersed in 30 mL of DI water. A 12 mL aliquot of this dispersion was then mixed with 80 mL ethanol and 4 mL ammonium hydroxide (25-28 wt%) under vigorous mechanical stirring for 1 min. This solution was warmed by using a water bath that was set to 50 ˚C. Subsequently, two aliquots of tetra-ethyl orthosilicate (TEOS) were added every 20 min. The volume of the first aliquot was 0.4 mL and the second aliquot was 0.2 mL. Eventually, the reaction products were collected by a NdFeB magnet and washed with ethanol three times. Each ethanol wash used a brief 2 min sonication (in order to completely re-disperse particles) and the followed by a magnetic separation step.

It is important to note that the second aliquot of TEOS was increased to 0.4 mL to generate the larger particles shown in **Figure S1** (particle batch #2).

3) Synthesis of $Fe_3O_4$@$SiO_2$@PEG nanoparticles

$Fe_3O_4$@$SiO_2$ nanoparticles were first modified with 3-(trimethoxysilyl)propyl methacrylate before coating with PEG. Briefly, a 3 mL aliquot of the particle ethanol dispersion was added to 80 μL of 3-(trimethoxysilyl) propyl methacrylate and 5 μL de-ionized water. The mixture was sonicated briefly for 1 min and then placed onto a temperature controlled shaker to shake for 48 hr at 37 ºC. The silane modified nanoparticles were firstly washed with ethanol once and then washed with DI water twice. The particles were finally dispersed in 3 mL DI water.

The 3 mL particle dispersion was boiled together with 100 mL de-ionized water for 5 min. The entire mixture was cooled down to 90 ºC afterwards. 1 mL poly(ethylene

glycol) methyl ether methacrylate (Mn~500), 0.3 mL poly(ethylene glycol) diacrylate (Mn~700), and 0.2 mL potassium persulfate solution (100 mM) were added consecutively. The reaction was conducted at 90 $^{o}$C for 3 hrs under $N_2$ flow. The reaction products were washed with DI water once and 75 mM potassium phosphate buffer (pH=6.4) twice. Finally, the particles were concentrated and redispersed in 1.5 mL of 75 mM potassium phosphate buffer (pH=6.4).

4) Hydrogel nanocomposite with MNPs for on-demand assembly

To synthesize MNP-DNA supramolecular hydrogel nanocomposites, 15 μL MNP dispersion of $Fe_3O_4$@$SiO_2$@PEG (in 75 mM potassium phosphate buffer) was directly mixed with 15 μL DNA solution (~3.3 mM in water) in an Eppendorf tube. The mixture was pre-heated to ~90 $^{o}$C in a water bath first, then a vortex mixer (~15 s mixing time) was used to create an homogeneous mixture. Note that mixture will rapidly gelate if cooled below 90 $^{o}$C transiently, and the sample must be heated again to ~90 $^{o}$C before handling and transferring to form the thin film. Two glass slides were pre-warmed to 90 $^{o}$C and a 30 μL drop of the warmed hydrogel was sandwiched and allowed to spread. The thickness of the hydrogel was controlled by using parafilm as a spacer. We used 4 layers of parafilm spacer for most of the experiments described in this paper as we found that thinner films formed weakly colored hydrogels.

For the MNP-polyacrylamide hydrogel nanocomposite, the polyacrylamide hydrogel was pre-made by using radical polymerization. 5 mg acrylamide, 33 μL pre-annealed DNA duplex 1 mM solution (the DNA duplex was acrylamide terminated on 5' end as crosslinker), 1 μL saturated solution of potassium persulfate, and 0.5 μL of N,N,N′,N′-tetramethylethylenediamine were mixed together and allowed to gelate at room temperature for 24h. The mixing step with the MNP solution was identical to the DNA supramolecular hydrogel solution. However, the mixing step required greater effort as the DNA crosslinked polyacrylamide hydrogel was not completely melted at 90 $^{o}$C.

DNA sequences for polyacrylamide crosslinking are listed as below:
Strand #1 /5'Acryd/TT TTT TTT TTG GTA GCG AGT TAG GGA GCC GA 3'
Strand #2 /5'Acryd/TT TTT TTT TTT CGG CTC CCT AAC TCG CTA CC 3'

**Characterization**

TEM images were acquired with a Hitachi HT-7700 with 80 kV accelerating voltage. Reflectivity spectra were measured with a FLAME-S-VIS-NIR Spectrometer equipped with a premium 400 μm reflection probe (Ocean optics Inc., Dunedin, FL). The spectrometer was calibrated with a diffuse reflectance standard (PTFE) prior to all the measurements. All the spectra data were recorded through the Ocean View 1.6.3 software package.

Rheological tests were carried out on an AR2000ex rheometer equipped with a temperature controller. The rheological experiments were performed on 25 mm parallel plates using 100 μL of particle-contained hydrogels (particle dispersion: DNA gel solution=1:1 by volume). The gap size was set with 0.12 mm. Frequency sweep tests

were carried out on mixtures between 0.01 Hz to 1000 Hz at 25 $^{o}$C at a fixed strain of 1%. Temperature sweep tests were carried out at 6.28 rad/s with specific temperature range based on specific sequence (for details see **Figure 2**).

The laser patterning imaging was performed using a Nikon Eclipse Ti microscope, operated with Nikon Elements software, a 1.49 NA CFI Apo 100x objective equipped with a perfect focus system and LED light source along with a laser excitation source. An RICM filter cube with a 535 nm excitation filter was employed to visualize particle alignment. Laser patterning was using a UGA-42 Firefly galvo mirror illumination system (Rapp OptoElectronic, Germany) with the ROE Syscon-NIS software (version 1.1.9.9, Rapp Optoelectric) to spatiotemporally control a 785 nm NIR laser at 50 mW power. The demonstration images (in Figure 4) were taken by Magic Zoom™ 1080p microscope camera.

## 1. TEM characterization of different sizes of MNPs

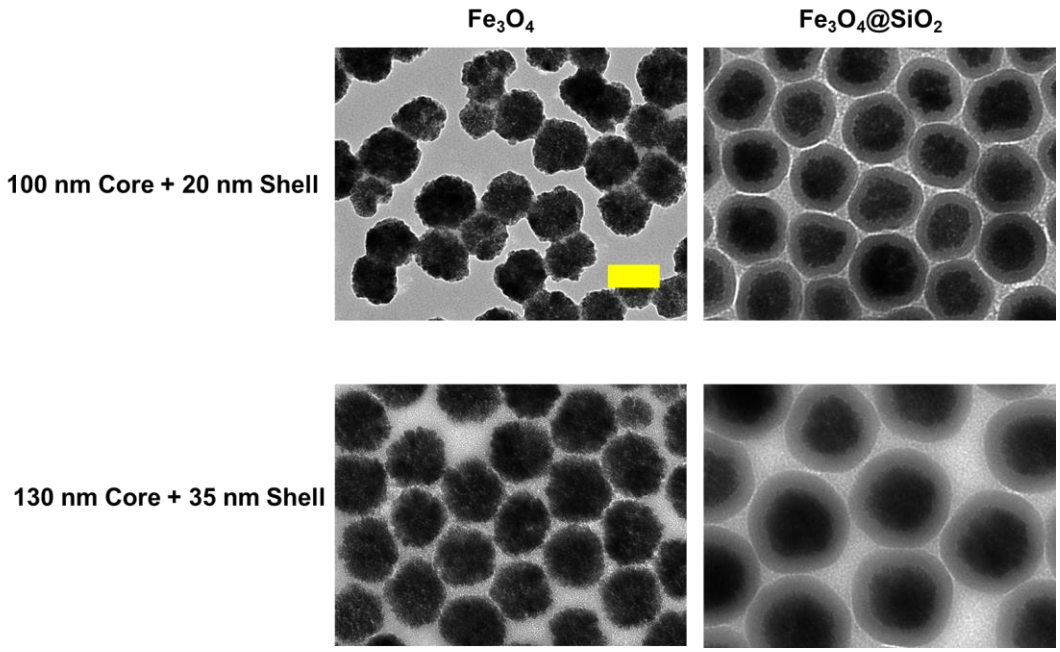


**Figure S1** TEM images of different sizes of MNPs. Upper set: MNPs with ~100 nm $Fe_3O_4$ core and ~20 nm shell. Lower set: MNPs with ~130 nm $Fe_3O_4$ core and ~35 nm shell. Scale bar: 100 nm.

## 2. Reflection spectra of photonic crystal structure assembled by $Fe_3O_4$@$SiO_2$@PEG nanoparticles

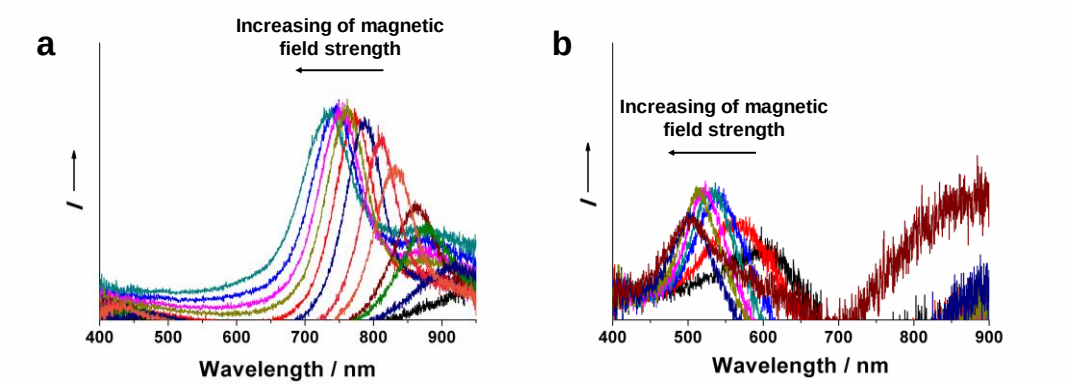


**Figure S2** Reflection spectra of photonic crystal structure that was magnetically assembled using $Fe_3O_4$@$SiO_2$@PEG nanoparticles. a) Reflection spectra of particle assembly in deionized water. b) Reflection spectra of particle assembly in 100 mM potassium phosphate buffer solution. Note that both spectra data were obtained under magnetic field strength ranging from 20 to 400 Gauss. Each color in the plots represent spectra measured using different strength of magnetic field. The presence of reflection peaks demonstrates the formation of MNP photonic crystal assemblies in buffer.

### 3. Dehybridization of DNA duplexes (modified on a glass surface) upon photothermal heating of $Fe_3O_4$@$SiO_2$ nanoparticles

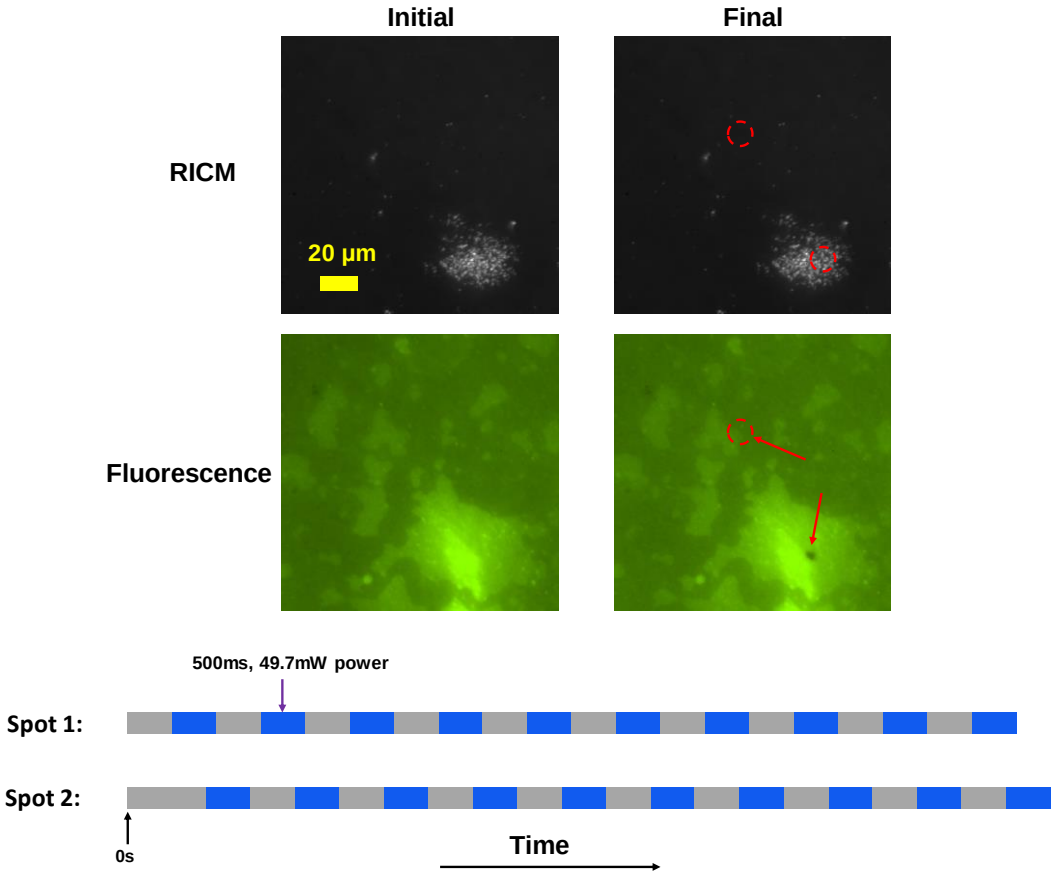


**Figure S3** A proof of concept experiment that demonstrates that photothermal heating of $Fe_3O_4$@$SiO_2$ nanoparticles generates sufficient heat to locally dehybridize DNA duplexes. In this experiment, one of the DNA strands was covalently anchored to a glass surface and the complementary strand was modified with fluorescein as a fluorescence indicator. The laser irradiation was performed on two different spots. Spot 1 did not have any MNP while spot 2 showed a number of particles based on RICM. Upon irradiation, spot 2 displayed a loss of fluorescence while spot 1 remained unchanged. This result indicates that the photothermal heating generated by $Fe_3O_4$@$SiO_2$ leads to dehybridization of DNA duplexes.

## 4. Finite element simulation of photothermal effect of MNPs

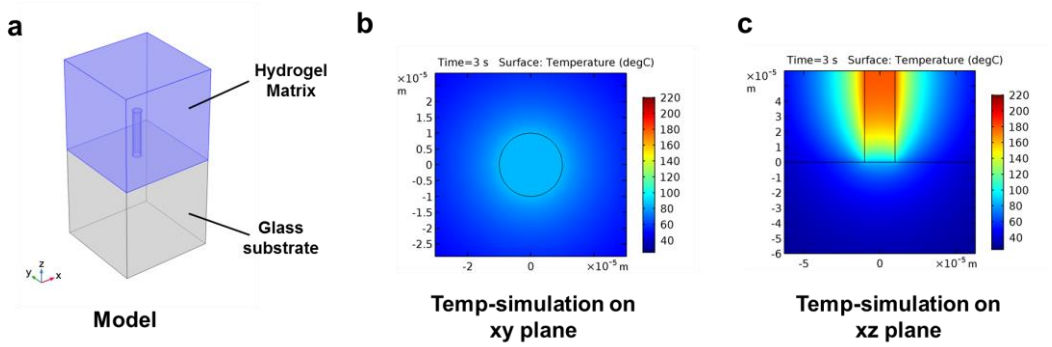


**Figure S4** Finite element simulation of photothermal heating using a 36.2 mW laser focused on a hydrogel. This simulation uses the model "heat transfer in solid" in COMSOL Multiphysics. a) Basic model of the simulation, in which the cylinder in the middle represents the path of the laser beam (radius=10 μm) and the blue box represents a limited area of hydrogel matrix while the grey box represents a limited area of glass substrate. The cylinder geometry (laser beam pathway) is treated as the heating source which has a power of 36.2 mW. b) A xy-plane cross-section that maps the temperature distribution after 3s of thermal energy generation. The units of the calibration bar is $^{o}$C. c) A xz-plane cross-section that maps the temperature distribution. The modeling indicates that the temperature increase produced by the photo-thermal effect exceeds the melting temperature of the DNA duplex (~60 $^{o}$C).

## 5. Rheology characterization of DNA hydrogels embedded with different sizes of MNPs

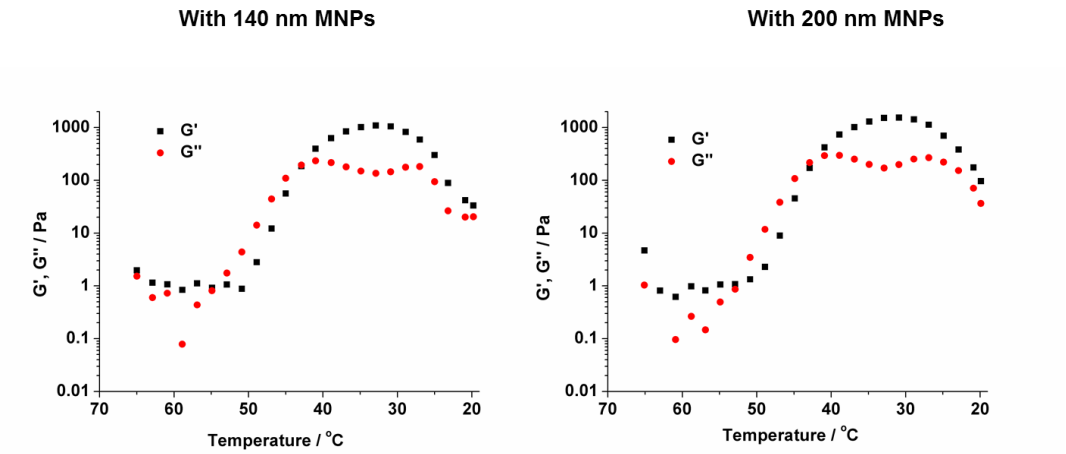


**Figure S5.** Plots showing temperature-dependent rheology measurements of DNA supramolecular hydrogels embedded with different sizes of MNPs. (Left: 140 nm MNPs; Right: 200 nm MNPs)

## 6. Rheology measurement of DNA duplex crosslinked polyacrylamide hydrogels

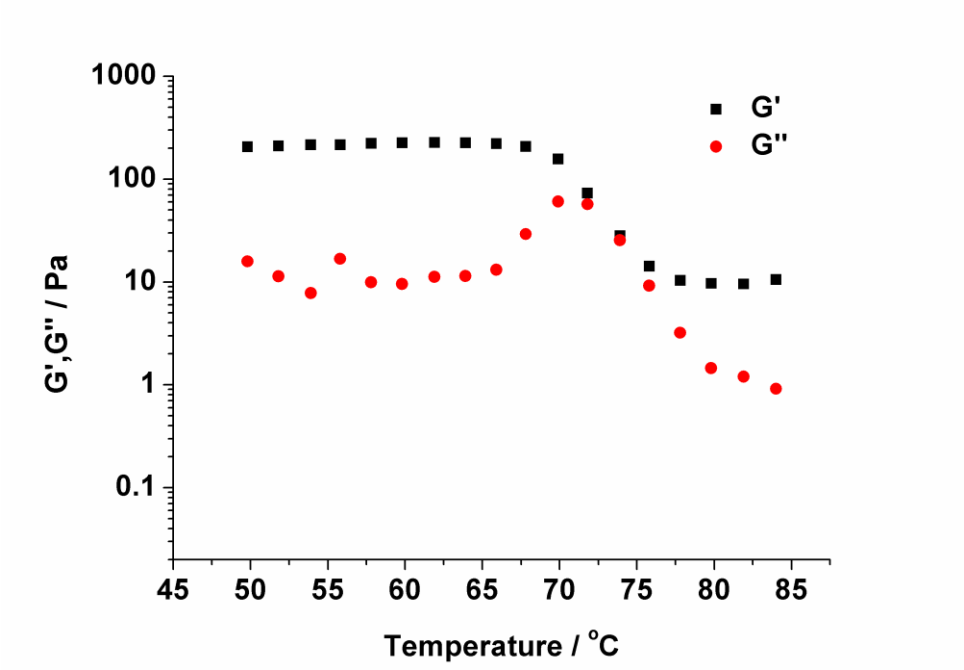


**Figure S6** Temperature-dependent rheology experiments with dsDNA crosslinked polyacrylamide hydrogels. The hydrogel (4 wt%) was mixed with MNPs at ~90 ºC with a volume ratio of 1:1. The protocol for preparation of the sample was similar to that used for pure DNA based PC hydrogels introduced in the main text.

## 7. Polyacrylamide-hydrogels crosslinked by DNA fail to facilitate MNP assembly under a magnetic field.

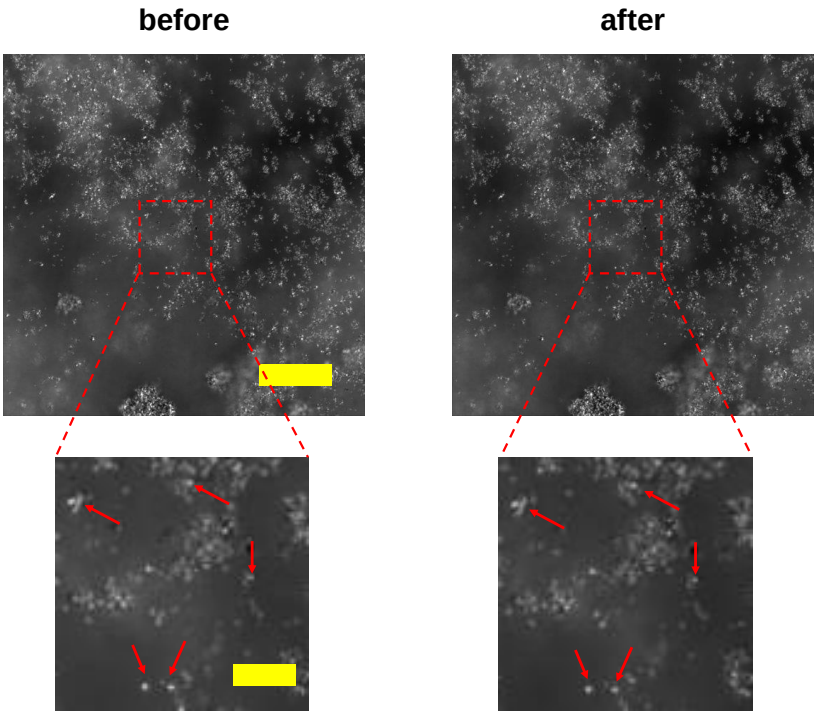


**Figure S7** In this experiment, we aimed to test whether the on demand assembly could be performed using polyacrylamide hydrogels that were crosslinked using DNA duplexes. These types of gels are commonly used in the literature, hence motivating this experiment. We found that these types of gels created barriers to the mobility of the MNPs even when the gel was heated using NIR illumination. We believe that this is because of polyacrylamide chain entanglement that hinder particle mobility. Thus, the all-DNA hydrogels discussed in our work are essential for on demand coloration. The conditions used for this experiment are identical to those used for the pure DNA supramolecular hydrogel shown in Figure 3. The microscopic results show nearly identical images before/after the sample was irradiated with 785 nm laser while applying a magnetic field. Note that the laser illumination was held for 3 sec while also applying a magnetic field of 100 Gauss at the same time. (Scale bar: 20 μm (upper set); 5 μm (lower set))

## 8. Photo patterning and erasing performed on DNA hydrogels with different sizes of MNPs

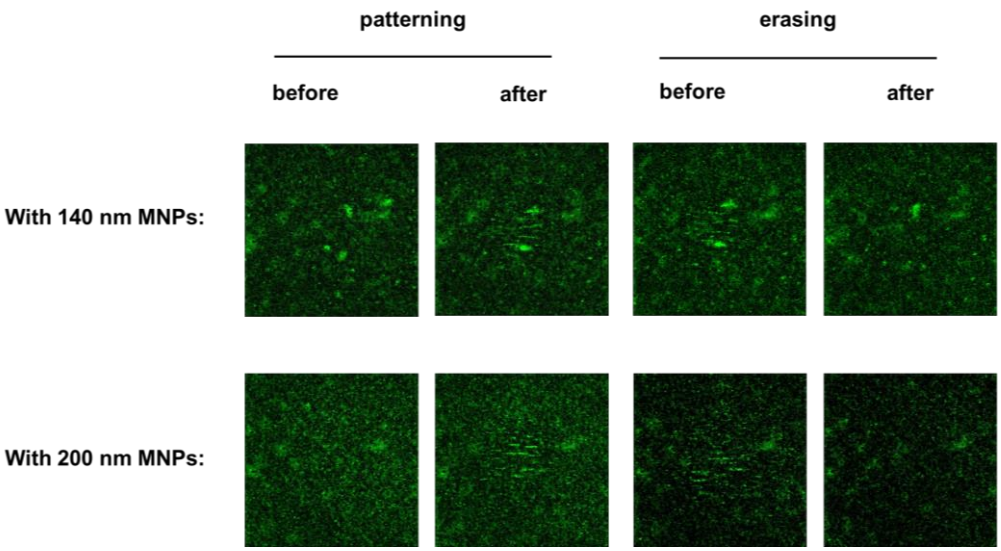


**Figure S8** Simultaneous NIR illumination and application of magnetic field leads to organization of MNPs into linear assemblies. This experiment was performed on DNA hydrogel loaded with the 140 nm and 200 nm diameter MNPs to confirm that the response is not sensitive to the size of the MNP for the sizes of particles tested in this work. Samples were illuminated with NIR for 3 sec while also applying a magnetic field ~100 Gauss to generate the patterns. MNP particle organization was lost when the samples were illuminated with NIR for 3 sec but without the application of the magnetic field. The methods used here are identical to that shown for main text Figure 3.

## 9. Examples of ridge detection

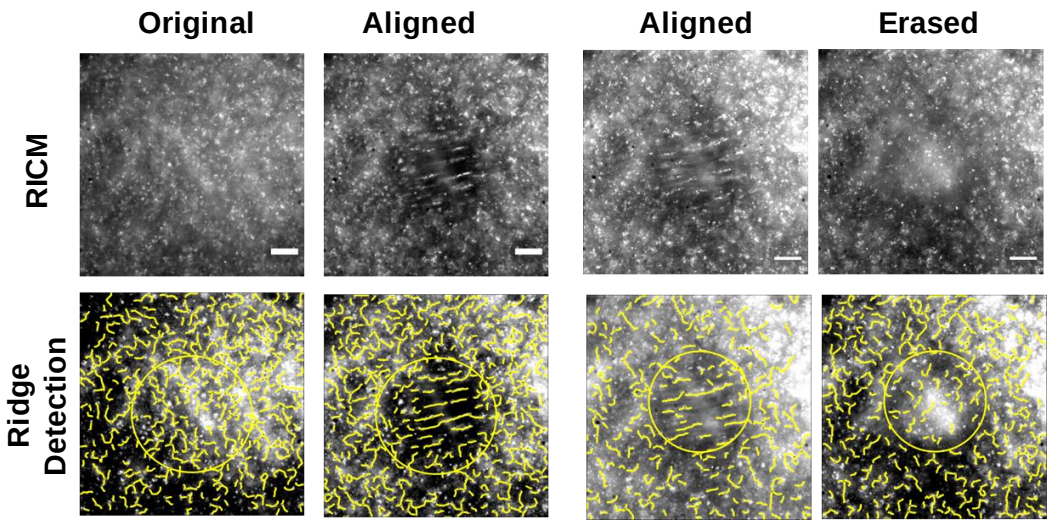


**Figure S9** Examples of analysis using the ridge detection plugin in ImageJ. Data was obtained in the circled area. Left: particle alignment; Right: particle de-alignment. (scale bar: 10 μm)

## 10. Model schematic of DNA-PC annealing following NIR illumination

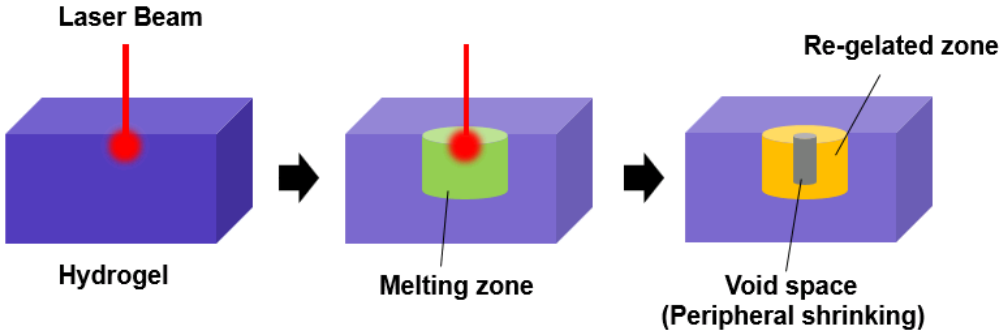


**Figure S10** Schematic of a possible explanation of the observed dark region formed at the illumination spot within the DNA-PC structures. We hypothesize that these regions arise from peripheral shrinking of the DNA hydrogel.

## 11. Characterization of peripheral region of illuminated areas in the DNA-PC hydrogel

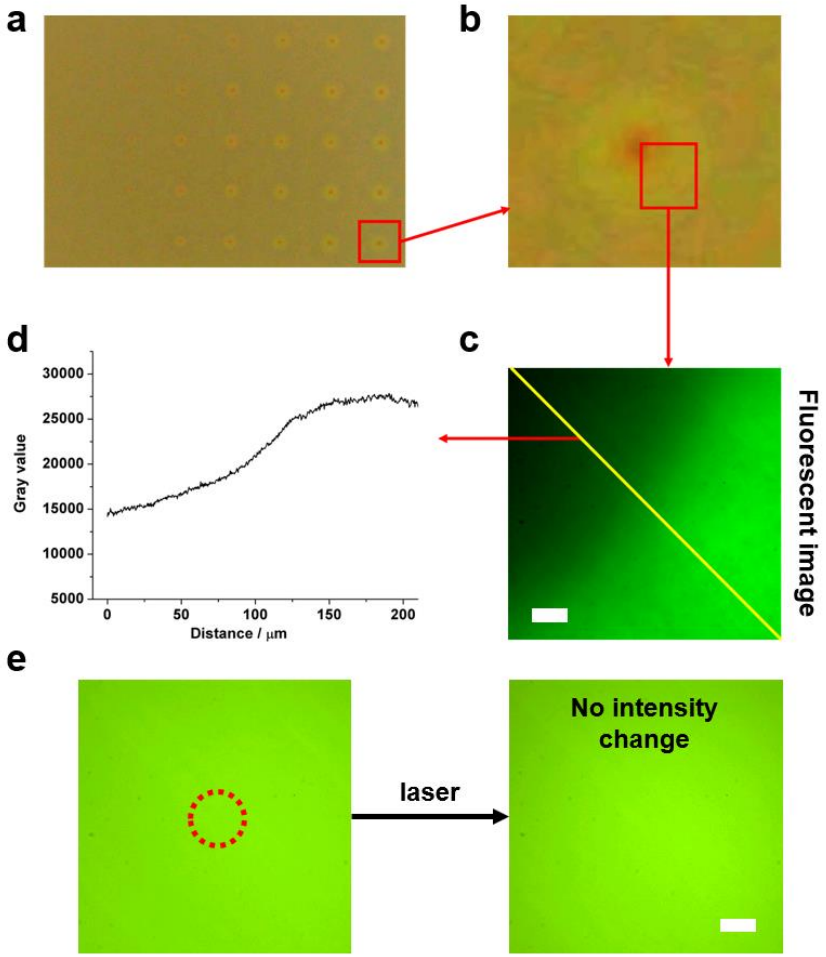


**Figure S11** Experimental evidence that supports the model illustrated in Figure S10. In this experiment, we used 6-carboxyfluorescein (FAM) labeled ssDNA to form the hydrogel in the same manner as described previously. a) and b) Typical spots that have a dark center in the middle. c) A fluorescence image that shows the intensity difference near the laser writing spot demonstrating reduced fluorescence. The dark area indicates a lower density of ssDNA. d) The intensity line scan plot in c). e) A control group without any MNPs. Since heating is produced by MNPs, removing the particles abolishes heating and local dehybridization of the DNA. This control group shows that photobleaching is minimal when illuminating with the 785 nm laser source. This is consistent with the spectral properties of FAM with its $\lambda_{max}$ = 495 nm. Scale bars: 20 μm.

**12. The role of particle concentration in tuning PC patterning.**

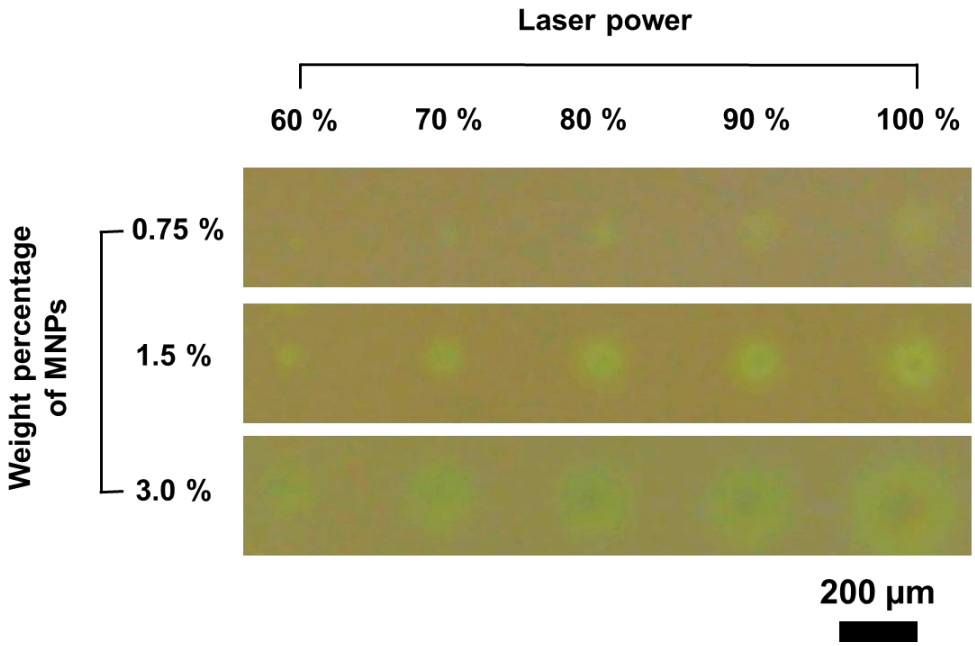


**Figure S12** Measurement of patterning area in DNA hydrogels as a function of the concentrations of MNP particles (200 nm diameter MNPs). The horizontal direction represents increasing laser powers. Vertical values represent the wt/wt% for MNPs doped DNA hydrogels.

**Table 1** Representative examples of re-writable technologies

| Coloration Mechanism | Writing trigger | Erase trigger | Writing time | Erasing time | Spatial resolution * | Ref. |
|---|---|---|---|---|---|---|
| Pigment/organic dye | Laser (405 nm) (without photomask) | Bulk heating | ~15min | ~2h | Medium | [2] |
| | UV light (with photomask) | Ozone or heat | 1-2min | ~5min-15min | High | [3-4] |
| | UV light (with hand-writing) | Vis light | ~20s | ~25s | Low | [5] |
| | Water | Dry air | N/A | ~22h | Medium | [6] |
| | pH (with hand-writing) | pH | N/A | ~15min | Low | [7] |
| Photonic crystal | Water (with hand-writing) | Dry air | ~5min | ~5-10min | Low | [8-9] |
| | Magnetic field | Magnetic field | ~1s | ~1s | Low | [10] |
| | UV light (with photo mask) | Vis light | ~2s | ~2s | Medium | [11] |
| Metal organic framework | Solar light (with photomask) | Darkness | ~1min | ~12h | High | [12] |
| This work | Laser (785 nm) | Laser or bulk heating | <1s | <1min (bulk heating)<br><10s (laser) | High | - |

* Spatial resolution: High <50 μm; Medium 50 μm< <1000 μm; Low >1000 μm

## References


1. Dong, Y.; Bazrafshan, A.; Pokutta, A.; Sulejmani, F.; Sun, W.; Combs, J. D.; Clarke, K. C.; Salaita, K., Chameleon-inspired strain-accommodating smart skin. *ACS Nano* **2019**, *13* (9), 9918-9926.
2. Müller, V.; Hungerland, T.; Baljozovic, M.; Jung, T.; Spencer, N. D.; Eghlidi, H.; Payamyar, P.; Schlüter, A. D., Ink-Free Reversible Optical Writing in Monolayers by Polymerization of a Trifunctional Monomer: Toward Rewritable "Molecular Paper". *Adv. Mater.* **2017,** *29* (27), 1701220.
3. Wei, J.; Jiao, X.; Wang, T.; Chen, D., Electrospun photochromic hybrid membranes for flexible rewritable media. *ACS Appl. Mater. Interfaces* **2016,** *8* (43), 29713-29720.
4. Wang, W.; Xie, N.; He, L.; Yin, Y., Photocatalytic colour switching of redox dyes for ink-free light-printable rewritable paper. *Nat. Commun.* **2014,** *5* (1), 1-7.
5. Wu, H.; Chen, Y.; Liu, Y., Reversibly photoswitchable supramolecular assembly and its application as a photoerasable fluorescent ink. *Adv. Mater.* **2017,** *29* (10), 1605271.
6. Sheng, L.; Li, M.; Zhu, S.; Li, H.; Xi, G.; Li, Y.-G.; Wang, Y.; Li, Q.; Liang, S.; Zhong, K., Hydrochromic molecular switches for water-jet rewritable paper. *Nat. Commun.* **2014,** *5* (1), 1-8.
7. Hariharan, P.; Pitchaimani, J.; Madhu, V.; Anthony, S. P., A halochromic stimuli-responsive reversible fluorescence switching 3, 4, 9, 10-perylene tetracarboxylic acid dye for fabricating rewritable platform. *Optical Materials* **2017,** *64*, 53-57.
8. Ge, J.; Goebl, J.; He, L.; Lu, Z.; Yin, Y., Rewritable photonic paper with hygroscopic salt solution as ink. *Adv. Mater.* **2009,** *21* (42), 4259-4264.
9. Du, X.; Li, T.; Li, L.; Zhang, Z.; Wu, T., Water as a colorful ink: transparent, rewritable photonic coatings based on colloidal crystals embedded in chitosan hydrogel. *J. Mater. Chem. C* **2015,** *3* (15), 3542-3546.
10. Wang, M.; He, L.; Hu, Y.; Yin, Y., Magnetically rewritable photonic ink based on superparamagnetic nanochains. *J. Mater. Chem. C* **2013,** *1* (38), 6151-6156.
11. Liu, J.; Wang, Y.; Wang, J.; Zhou, G.; Ikeda, T.; Jiang, L., Inkless Rewritable Photonic Crystals Paper Enabled by a Light-Driven Azobenzene Mesogen Switch. *ACS Appl. Mater. Interfaces* **2021,** *13* (10), 12383-12392.
12. Garai, B.; Mallick, A.; Banerjee, R., Photochromic metal–organic frameworks for inkless and erasable printing. *Chem. Sci.* **2016,** *7* (3), 2195-2200.